



X-ray spectra, variability and pair wind models of Seyfert 1 nuclei
by Karen Marie Leighly

A thesis submitted in partial fulfillment of the requirements for the degree of Doctor of Philosophy in
Physics

Montana State University

© Copyright by Karen Marie Leighly (1991)

Abstract:

Previously, iron features were not known to be a common feature of the X-ray spectra of Active Galactic Nuclei (AGN). The data from a long observation of NGC 5506 performed by EXOSAT were reanalyzed, and an emission line and an absorption edge were found. Subsequently, 47 X-ray spectra from a sample of 40 AGN observed with EXOSAT were reanalyzed. Evidence for line emission was found in 13 spectra from 12 sources; however, the line intensities were not well determined.

X-ray variability is an interesting feature of some low luminosity Seyfert 1 galaxies. As part of Tsuruta's simultaneous multi-frequency campaign, the Seyfert I nuclei NGC 7469. and NGC 6814 were observed with the LAC onboard Ginga. These data were analyzed along with a second Ginga observation of NGC 6814. The flux level of NGC 7469 was low and the satellite pointing was not stable, making detailed analysis difficult. The flux level was seen to decrease during the second day of observation with a halving time scale of 25,000 seconds. The photon index was remarkably flat.

From the two observations of NGC 6814, a wealth of interesting results emerged. The rapid flux variability with time scale of ~ 300 seconds and the 12000 second periodicity characteristic of this unusual source were confirmed in both observations. During the first observation, periodic dips were found, in which the flux fell to nearly zero. Spectral variability was confirmed during these dips, as well as a decrease in line emission. During the second observation, periods of rapid flux increase and decrease were found, and spectral variability was again found. Well defined energy delays were also discovered. A variable absorption model was explicitly fit to the delay data. This model could successfully though qualitatively explain the spectral variability during the regions of fastest variability.

In the intense radiation field of an AGN, the motion of particles is influenced by the gravitational and radiation fields. To explore the motion of such particles, a spherically symmetric model by Abramowicz et al. 1990 was extended to a more realistic case by using a modified radiation stress energy tensor. This modification produced a significant change in the character of the critical point solutions.

X-RAY SPECTRA, VARIABILITY AND PAIR WIND MODELS
OF SEYFERT 1 NUCLEI

by

Karen Marie Leighly

A thesis submitted in partial fulfillment
of the requirements for the degree

of

Doctor of Philosophy

in

Physics

MONTANA STATE UNIVERSITY
Bozeman, Montana

November 1991

© COPYRIGHT

by

Karen Marie Leighly

1991

All Rights Reserved

D378
L5335

APPROVAL

of a thesis submitted by

Karen Marie Leighly

This thesis has been read by each member of the thesis committee and has been found to be satisfactory regarding content, English usage, format, citations, bibliographic style and consistency, and is ready for submission to the College of Graduate Studies.

11-8-91
Date

Richard Teut
Chairperson, Graduate Committee

Approved for the Major Department

11-8-91
Date

John Hermonstein
Head, Major Department

Approved for the College of Graduate Studies

November 11, 1991
Date

Henry J. Parsons
Graduate Dean

STATEMENT OF PERMISSION TO USE

In presenting this thesis in partial fulfillment of the requirements for a doctoral degree at Montana State University, I agree that the Library shall make it available to borrowers under rules of the Library. I further agree that copying of this thesis is allowable only for scholarly purposes, consistent with "fair use" as prescribed in the U.S. Copyright Law. Requests for extensive copying or reproduction of this thesis should be referred to University Microfilms International, 300 North Zeeb Road, Ann Arbor, Michigan 48106, to whom I have granted "the exclusive right to reproduce and distribute copies of the dissertation in and from microfilm and the right to reproduce and distribute by abstract in any format."

Signature Karen Leighly
Date 11/8/91

ACKNOWLEDGEMENTS

Primary acknowledgement and thanks must go to Sachiko Tsuruta for her patience and help during my years as her student. Her support, both financial through NASA grants, and otherwise, has gone far beyond that expected from a research advisor.

Thanks are due to Ken Pounds and the rest of the Leicester group for their hospitality during my two visits for EXOSAT data analysis. Special thanks are due to T. Jane Turner, Tahir Yaqoob, Ian George and Paul Nandra.

Many thanks are due to Hideyo Kunieda and the rest of the Nagoya group for their hospitality during my two visits for *Ginga* data analysis. Particular thanks go to Hisamitsu Awaki for his extensive help and friendship.

Acknowledgement and thanks go to Christine Done for allowing me to use her time series analysis software.

The people who have helped me at Montana State University are innumerable. Matthew Benacquista must be thanked for helping me to understand general relativity at least a little. All of the graduate students must be thanked for their friendship, especially Stuart Hutton, Rand Swanson, Brad Tritz and Hideyuki Umeda. The faculty have been helpful, and must be thanked for their patience and support. Particular thanks go to John Hermanson and Georgeanne Caughlan.

Many thanks are due to my parents, Hollis P. Leighly and Elizabeth P. Leighly, and my brother, David P. Leighly. Their support and confidence have helped me an immeasurable amount. Last but certainly not least, more than thanks must go to Corin L. Dreykus, without whom I could have never done it.

The work in this thesis would not have been possible without the help of many people, and it is impossible to thank them all individually here.

TABLE OF CONTENTS

	Page
1. INTRODUCTION.....	1
General.....	1
Plan of the Thesis.....	4
2. X-RAY SPECTRA OF SEYFERT GALAXIES.....	8
General.....	8
X-Ray Power Law Emission.....	8
Low Energy Absorption.....	10
Soft Excess Emission.....	13
Iron Emission and Absorption.....	15
Hard X-ray Hump.....	20
3. THE EUROPEAN X-RAY OBSERVATORY SATELLITE.....	27
The EXOSAT Mission.....	27
General.....	27
The ME Experiment.....	28
The LE Experiment.....	31
Data Analysis and Spectral Fitting.....	31
Background Subtraction.....	31
The ME Experiment.....	31
The LE Experiment.....	32
Spectral Fitting.....	33
4. IRON EMISSION AND ABSORPTION FEATURES IN EXOSAT X-RAY SPECTRA.....	35
The Long Observation of NGC 5506.....	35
Results.....	36
Data Reduction.....	36
Spectral Fitting.....	37
Discussion.....	42
The EXOSAT Spectral Survey Sources.....	44
Data Reduction and Analysis.....	45
Results.....	54
Iron Line Fitting.....	54
Iron Absorption Edge Fitting.....	63
Combined Fitting.....	67
Statistical Analysis.....	67
Discussion.....	74

TABLE OF CONTENTS—Continued

	Page
5. VARIABILITY OF X-RAYS FROM SEYFERT NUCLEI	77
Intensity Variability of X-Rays	77
Observations	77
Models	80
Spectral Variability	82
Absorption Column Variability	83
Variability of Cold Column	83
Warm Absorber	84
Variability in Relative Normalization of Separate Spectral Components	87
Spectral Variability Due to Compton Effects	89
Spectral Variation by Partial Covering	93
6. THE GINGA X-RAY SATELLITE	96
General	96
The Large Area Counter	98
Design Characteristics	98
Calibration	99
X-Ray Background	101
Data Analysis	103
General	103
Data Selection and Background Subtraction	103
Spectral Fitting	106
Time Series Analysis	107
7. THE GINGA OBSERVATION OF NGC 7469	112
Simultaneous Observations of Seyfert Galaxies	112
Results From Previous Observations	113
Results	115
The <i>Ginga</i> Observation	115
Time Series Analysis	117
Spectral Analysis	129
Discussion	142
Low Activity	142
Flux Variability	143
Flat Spectral Index	143
Soft Excess	145
Short Term Spectral Variability	147
Model Speculations	147

TABLE OF CONTENTS—Continued

	Page
8. THE <i>GINGA</i> OBSERVATIONS OF NGC 6814	150
Simultaneous Observations of Seyfert Galaxies Continued	150
Results from Previous Observations	150
Results	153
The <i>Ginga</i> Observations	153
Periodicity	160
Spectral Analysis – Entire Observation	180
Fastest Variability	193
Correlation Plot Analysis	194
Cross Correlation Analysis	202
Template Fitting Analysis	208
Spectral Analysis	219
Model Calculations	231
The Variable Absorption Model	233
Fitting the Model	234
Light Curves Predicted by the Model	238
Spectra Predicted by the Model	240
Implications of the Model on Physical Parameters	247
Discussion	249
Similarities Between the April and October Results	250
Implications of Model for April Data	252
Implications of Realistic Geometries	253
Implications of the Absorption Model on the Hardness Variability	255
Competing Models	257
9. SOME ASPECTS OF OPTICALLY THIN WINDS FROM AGN	260
Background	260
Results	262
Derivation of the Wind Equation	263
The Radiation Stress Energy Tensor	266
Extended case	266
Shell case	269
Solutions	271
Discussion	289

TABLE OF CONTENTS—Continued

	Page
10. CONCLUSIONS	290
Results, Conclusions and Unfinished Work	290
Future Prospects of X-ray Astronomy	295
REFERENCES CITED	298
APPENDICES	306
Appendix A—Supplementary Light Curves for Chapter 8	307
Appendix B—Spectral Fits for Chapter 8	322

LIST OF TABLES

Table	Page
1. Spectral fitting results from the EXOSAT long observation of NGC 5506	38
2. Observation log of the EXOSAT spectral survey sources	46
3. Iron line spectral fitting results from the EXOSAT spectral survey sources	49
4. Iron absorption edge spectral fitting results from the EXOSAT spectral survey sources	55
5. Iron line and edge spectral fitting results from the EXOSAT spectral survey sources	68
6. Observing log from the <i>Ginga</i> observation of NGC 7469	116
7. Orbit spectral fitting results for NGC 7469	130
8. Spectral fitting results for the final combined spectra	133
9. Mean SSUD count rates in the source and background data	140
10. The results of spectral fitting to the folded October data	191
11. The results of fitting to the cross correlation of the April dip data	205
12. Comparison of lags calculated using CCF and template fitting	206
13. Fit results for the arctangent template	211
14. The results of spectral fitting to the combined April dip data	220
15. The results of spectral fitting to the combined spectra from the October ingress and egress data	227
16. Fit results for the ingress and egress data	236
17. Fitting results to the measured and simulated data	246

LIST OF FIGURES

Figure	Page
1. Absorbed spectra.....	12
2. Partial covering spectrum.....	22
3. Reflection spectrum	24
4. Power law fitting to NGC 5506 data.....	39
5. Power law plus line and edge fitting to NGC 5506 data.....	41
6. Power law fit plus residuals from NGC 3227.....	61
7. Power law plus an iron emission line fit plus residuals from NGC 3227	62
8. Power law plus absorption fit for ESO 103-G35	66
9. Line and edge fit for NGC 5506.....	69
10. Line and edge fit for MCG-6-30-15.....	70
11. Schematic view of the <i>Ginga</i> satellite	97
12. The efficiency of detection as a function of energy of the LAC.....	100
13. Light curve for NGC 7469 in the energy range 1.2-20.9 keV.....	118
14. Trend in total flux for NGC 7469	121
15. Soft, medium and hard light curves for the first day of observation	123
16. Soft, medium and hard light curves for the second day of observation	124
17. Softness and hardness ratios for the first day of observation	126
18. Softness and hardness ratios for the second day of observation.....	127

LIST OF FIGURES—Continued

Figure	Page
19. Power law fit to FINAL6T.....	134
20. Power law plus line fit to FINAL6T.....	135
21. Spectrum FNL6T.....	137
22. Spectrum FNLQ6T.....	138
23. April total light curve.....	155
24. October total light curve.....	157
25. Light curve and hardness ratio from the first day of the April observation.....	158
26. Light curve and hardness ratio from the second day of the April observation.....	159
27. Light curve and softness ratio for the October data.....	161
28. Autocorrelation of April data, in the energy band 1.11–20.9 keV.....	163
29. Number of UDCF's contributing to the correlation sum, for the April data.....	164
30. Periodograms for the April data, in the energy band 1.11–20.9 keV.....	165
31. Autocorrelation of October data, in the energy band 1.11–20.9 keV.....	167
32. Number of UDCF's contributing to the correlation sum, for the October data.....	168
33. Periodograms for the October data, in the energy band 1.11–20.9 keV.....	169
34. Autocorrelation of October data hardness ratio.....	174
35. Periodogram for October data hardness ratio.....	175
36. Folded light curve for the April data.....	177
37. Folded light curve for the October data.....	178
38. Folded light curve for the October data hardness ratio.....	179

LIST OF FIGURES—Continued

Figure	Page
39. Folded light curve of photon index, for the October observation	184
40. Line flux versus continuum flux correlation plot of April data	185
41. Line flux versus continuum flux correlation plot of October data.....	186
42. Photon index versus continuum flux correlation plot of April data	188
43. Photon index versus continuum flux correlation plot of October data	189
44. χ^2 contours of folded spectra from the October observation	192
45. Soft versus medium energy flux correlation plot for April data, around dips	195
46. Hard versus medium energy flux correlation plot for April data, around dips	196
47. Hard versus medium energy flux correlation plot for the ingress section of the October data	198
48. Medium versus soft energy flux correlation plot for the ingress section of the October data	199
49. Hard versus medium energy flux correlation plot for the egress section of the October data	200
50. Medium versus soft energy flux correlation plot for the egress section of the October data	201
51. Example cross correlation from October ingress data	204
52. Template fitting to total ingress light curve	212
53. Template fitting to softer ingress light curves.....	213
54. Template fitting to harder ingress light curves.....	214
55. Template fitting to total egress light curve	215
56. Template fitting to softer egress light curves	216
57. Template fitting to harder egress light curves	217

LIST OF FIGURES—Continued

Figure	Page
58. N_H versus photon index χ^2 contours from the first dip of the April data	223
59. N_H versus photon index χ^2 contours from the second dip of the April data	224
60. N_H versus photon index χ^2 contours from the third dip of the April data	225
61. The ingress spectrum OIHRD3 from the October data	229
62. The ingress spectrum OHLT5I from the October data	230
63. χ^2 contour for OHLT5I, and χ^2 line for OIHRD3	232
64. Best fit of exponential model to the ingress section of the October data	237
65. Best fit of exponential model to the egress section of the October data	237
66. Model spectra of the ingress section of the October data	243
67. Model spectra of the egress section of the October data	244
68. Saturation velocity profiles for the shell case	272
69. Saturation velocity profiles for the extended case	274
70. Integrated velocity profiles for the case $A = 0$	275
71. Integrated velocity profiles for the shell case with $A = 3$	276
72. Integrated velocity profiles for the shell case with $A = 5.7$	277
73. Integrated velocity profiles for the shell case with $A = 6.9$	278
74. Integrated velocity profiles for the shell case with $A = 8$	279
75. Integrated velocity profiles for the shell case with $A = 28$	280
76. Integrated velocity profiles for the shell case with $A = 1000$	281
77. Integrated velocity profiles for the extended case with $A = 1.5$	282

LIST OF FIGURES—Continued

Figure	Page
78. Integrated velocity profiles for the extended case with $A = 2.7$	283
79. Integrated velocity profiles for the extended case with $A = 5.5$	284
80. Integrated velocity profiles for the extended case with $A = 1000$	285
81. Light curve of first dip from the April observation.....	308
82. Light curve of second dip from the April observation.....	309
83. Light curve of third dip from the April observation.....	310
84. Light curve of April data from 0 to 15,000 seconds in four different energy bands.....	311
85. Light curve of April data from 85,000 to 100,000 seconds in four different energy bands.....	312
86. Light curve of April data from 100,000 to 115,000 seconds in four different energy bands.....	313
87. Light curve of October data from 0 to 15,000 seconds in four different energy bands.....	314
88. Light curve of October data from 15,000 to 30,000 seconds in four different energy bands.....	315
89. Parameter light curve for April data from 0 to 1400 seconds.....	316
90. Parameter light curve for April data from 85,000 to 100,000 seconds.....	317
91. Parameter light curve for April data from 100,000 to 115,000 seconds.....	318
92. Parameter light curve for October data from 0 to 10,000 seconds.....	319
93. Parameter light curve for October data from 10,000 to 20,000 seconds.....	320
94. Parameter light curve for October data from 20,000 to 30,000 seconds.....	321
95. Spectral fit for ADIP, the combined dip spectrum.....	323
96. Spectral fit for A1D10, the first spectrum before the first dip.....	324

LIST OF FIGURES—Continued

Figure	Page
97. Spectral fit for A1DB3, the second spectrum before the first dip	325
98. Spectral fit for A1DA1, the spectrum after the first dip	326
99. Spectral fit for A2DBFR, the spectrum before the second dip	327
100. Spectral fit for A2DA3, the first spectrum after the second dip	328
101. Spectral fit for A2D3, the second spectrum after the second dip	329
102. Spectral fit for A3DB2, the spectrum before the third dip	330
103. Spectral fit for A3DA1, the spectrum after the third dip	331
104. Spectral fit for OI1 from the October ingress data	332
105. Spectral fit for OI3 from the October ingress data	333
106. Spectral fit for OI5 from the October ingress data	334
107. Spectral fit for OI7 from the October ingress data	335
108. Spectral fit for OIHRD3 from the October ingress data	336
109. Spectral fit for OHLT5I from the October ingress data	337
110. Spectral fit for O5E1 from the October egress data	338
111. Spectral fit for OE6 from the October egress data	339
112. Spectral fit for OE8 from the October egress data	340

ABSTRACT

Previously, iron features were not known to be a common feature of the X-ray spectra of Active Galactic Nuclei (AGN). The data from a long observation of NGC 5506 performed by EXOSAT were reanalyzed, and an emission line and an absorption edge were found. Subsequently, 47 X-ray spectra from a sample of 40 AGN observed with EXOSAT were reanalyzed. Evidence for line emission was found in 13 spectra from 12 sources; however, the line intensities were not well determined.

X-ray variability is an interesting feature of some low luminosity Seyfert 1 galaxies. As part of Tsuruta's simultaneous multi-frequency campaign, the Seyfert 1 nuclei NGC 7469 and NGC 6814 were observed with the LAC on-board *Ginga*. These data were analyzed along with a second *Ginga* observation of NGC 6814. The flux level of NGC 7469 was low and the satellite pointing was not stable, making detailed analysis difficult. The flux level was seen to decrease during the second day of observation with a halving time scale of 25,000 seconds. The photon index was remarkably flat.

From the two observations of NGC 6814, a wealth of interesting results emerged. The rapid flux variability with time scale of ~ 300 seconds and the 12000 second periodicity characteristic of this unusual source were confirmed in both observations. During the first observation, periodic dips were found, in which the flux fell to nearly zero. Spectral variability was confirmed during these dips, as well as a decrease in line emission. During the second observation, periods of rapid flux increase and decrease were found, and spectral variability was again found. Well defined energy delays were also discovered. A variable absorption model was explicitly fit to the delay data. This model could successfully though qualitatively explain the spectral variability during the regions of fastest variability.

In the intense radiation field of an AGN, the motion of particles is influenced by the gravitational and radiation fields. To explore the motion of such particles, a spherically symmetric model by Abramowicz et al. 1990 was extended to a more realistic case by using a modified radiation stress energy tensor. This modification produced a significant change in the character of the critical point solutions.

CHAPTER 1

INTRODUCTION

General

Active Galactic Nuclei (AGNs) are the bright nuclei of some galaxies. They are some of the most energetic objects in the universe. Their energy spectra are characteristically non-thermal; that is, the energy spectrum cannot be adequately described by a sum of stellar spectra. They emit nearly equal amounts of energy in all wave bands, and are a strong source of X-rays. There are many different kinds of AGN, and because they are so well studied in the optical wave band, the classification generally depends on their optical properties.

In this thesis, Seyfert 1 nuclei are the predominant type of AGN studied. These are characterized by a strong non-thermal infrared to X-ray continuum and broad optical emission lines from a wide range of ionizations. Generally the host galaxy can be optically resolved. However, Quasi-stellar Objects (QSOs), Seyfert type 2 nuclei, Narrow Emission Line Galaxies (NELGs), and Low Ionization Nuclear Emission Line Regions (LINERS) are also included, as well as a variety of Seyferts whose type are somewhere in between 1 and 2 (1.2, 1.9, for example) depending on the relative strength of the broad and narrow components of their emission lines (Turner 1988). In general many of the differences between these types are in their optical properties. Some differ in luminosity. For example,

QSOs are more luminous than Seyfert 1 nuclei, having a typical bolometric luminosity of $10^{44-47} \text{ erg s}^{-1}$ compared with $10^{41-44} \text{ erg s}^{-1}$ for Seyfert 1s. However, many of these AGN objects seem to have quite similar X-ray properties, perhaps indicating that the primary emission mechanism is the same.

It has been pointed out that the largest amount of energy from many AGN is emitted from the central region. Since the discovery of this fact, the source of power for this emission has been debated. The currently most popular idea for the predominant source of power is the accretion of material onto a supermassive black hole having a mass from 10^6-10^9 solar masses. The form of the accretion flow is generally thought to depend on the accretion rate (e.g. Rees 1984). Rapid X-ray variability from a fraction of low luminosity Seyfert 1 nuclei implies that the X-rays may be produced in a small central region, from 5 to $100 r_s$, where r_s is the Schwarzschild radius appropriate for the supermassive black hole. The broad emission lines are in general thought to come from a region larger than $100 r_s$, from clouds which have been photoionized by the strong high energy continuum from further inside.

Many AGN, and in particular, Seyfert 1 nuclei have been detected in X-rays. Recent analysis of maneuvering data from the Japanese *Ginga* X-ray satellite from 3 years of operation found 93 Seyfert galaxies detected (Awaki 1991). In this study, it was estimated that 139 optically identified Seyfert 1 galaxies came into the field of view. Pointing observation data from 75 Seyfert galaxies from the *Einstein Observatory* Imaging Proportional Counter has been recently analyzed by Kruper, Urry and Canizares (1990). Many more detections in X-rays are expected from more sensitive detectors such as those used by the X-ray satellite *ROSAT* in the recently completed All Sky Survey. X-ray emission from at least a portion of Seyfert galaxies has been frequently observed.

As will be discussed in Chapter 2, the primary X-ray radiation from Seyfert 1 galaxies seems to be non-thermal. However, there are spectral features imprinted on the non-thermal primary spectrum which may be thermal, or which come from reprocessing of X-rays in cold material. Therefore, the careful study of the X-ray spectra from Seyfert 1 galaxies can give information about both the nature of the primary spectrum and the material surrounding the emission region.

A fraction of Seyfert 1 nuclei have been found to be rapidly variable, with a doubling time scale of as small as 100 seconds. There is some evidence that the time scale of variability is characteristic of the primary emission process, since luminosity and the time scale of variability have been found to be correlated (Barr and Mushotzky 1986; McHardy 1989). The most naive estimation of the size of the X-ray emission region comes from the light crossing time scale, and can be found from the relation $R = c\Delta T$. In many of the fastest variable AGN, this region is found to be as small as 10^{12} cm. Much information about the nature of the emission process and the material around the Seyfert 1 can be gained by studying in detail the variability of AGN. Of particular interest is spectral variability, because of the strong constraints which can be placed on models of the emission region.

Coupled with the observations of Seyfert 1 nuclei are the theories of the emission region and of the material surrounding the emission region. As mentioned above, copious X-rays have been observed from many Seyfert 1 galaxies, and the rapid variability implies that the emission region must be very small. Therefore, close to the emission region, the flux of radiation will be very intense. Under such radiation flux, some particles may not be gravitationally bound to AGN, and so particle winds may result. Therefore, it is interesting to investigate the nature of such a wind.

Plan of the Thesis

The remainder of this thesis is divided into nine chapters. Two of these chapters, Chapters 2 and 5, provide review of spectra and variability of Seyfert 1 nuclei. Two others, Chapters 3 and 6 provide descriptions of the instrumentation and satellites used to obtain the data under investigation. Three of the chapters, Chapters 4, 7 and 8 describe details of the data analysis conducted by the author, and interpretation of the results. One chapter, Chapter 9, describes her purely theoretical calculation describing the motion of particles in a radiation field. The final chapter is the conclusion.

Chapter 2 gives a partial review of the form of the X-ray spectral components found in Seyfert 1 nuclei. At least five separate spectral components have been identified. This chapter was written from the observer's point of view. Some theories of emission are briefly discussed.

Chapter 3 describes the European X-ray Observatory Satellite, and particularly the Medium Energy instrument. This description of the instrumentation is included for several reasons. The main reason is that it is unwise to use X-ray data without understanding the limitations of the instrument which collected it. Such use can lead to over-interpretation of results. But also, the understanding of the instrument provides a depth and richness to the data analysis. Also included in this chapter are details of the background subtraction for future reference, and also a short review of the statistics involved in fitting X-ray spectra.

Chapter 4 describes all of the EXOSAT data analysis done by the author. The first part describes the analysis and results of a long observation of NGC 5506. The purpose of this analysis was a search for iron emission and absorption features at ~ 7 keV. The long observation was used because of the better statistics which

it could provide. A comparison with a *Ginga* observation was also included, and some discussion of possible models is given.

The second part of Chapter 4 describes the reanalysis of the EXOSAT spectral survey sources. Again the intent of the reanalysis was the search for iron features. Since these observations were in general shorter in duration, the criteria for detection were necessarily statistical. A comparison with recent *Ginga* data from Awaki 1990 is also given. Some statistical correlations are performed on the sample of iron line detections.

Chapter 5 gives a review of X-ray variability of Seyfert 1 nuclei. First the description and nature of the flux variability is described. Several possible models for the most common kind of variability found are briefly discussed. The remainder of the chapter discusses spectral variability. This review was included for reference, because all three of the *Ginga* observations described in subsequent chapters indicated spectral variability. The most common type of spectral variability found is flux correlated. That is, in general, the X-ray spectra are usually observed to become softer as the X-ray flux increases. Thus this section describes models of spectral variability and shows how they can result in apparent flux correlated spectral variability. Diagnostics are described which can ideally decide which model of spectral variability is appropriate.

Chapter 6 describes the Japanese X-ray observatory satellite *Ginga*, as well as the Large Area Counter, the main instrument on-board *Ginga*. Data selection, and background subtraction and modeling are discussed in some detail, since there was a background subtraction problem in one of the *Ginga* observations. Finally in this chapter are described some relatively new methods, not yet widely used, for time series analysis of data with gaps.

In Chapter 7 the analysis, results and interpretation by the author of an observation of NGC 7469 are discussed. This observation found the source in a low flux state. Also there were pointing problems of the satellite further decreasing the flux. Because of the low flux, a background subtraction problem was encountered. The analysis of this problem and two possible solutions are described. Finally, the results of the time series and spectral analysis are compared with previous observations of this source, and a possible model is described.

Chapter 8, the longest chapter of the thesis, also describes the most significant and important work of this thesis. Results from detailed time series and spectral analysis of two *Ginga* observations of NGC 6814 are given. New results, never observed before from Seyfert 1 nuclei, or from this source, were found. Specifically, the hardness ratio from one of the observations was found to have 12,000 periodicity. Periodic dips to nearly zero flux from the other observation were observed. In addition, fast spectral variability, within a few hundred seconds, was discovered during both observations. Also, during one of the observations, energy lags were found, in the sense that the hard flux lagged the soft flux during flux decreases, while the soft flux lagged the hard flux during flux increases. Also shown are calculations from a new variation of the partial covering model explicitly fit to the time series results which successfully though qualitatively describes the spectral fitting results. Extensions of this simple model to explain the rest of the new observations are described.

Chapter 9 describes briefly the author's calculation of wind velocity profiles from AGN. In this calculation the particle approach has been taken; that is, the motion of the wind is interpreted to be the motion of non-interacting particles. Work has been done extending this to the fluid approach, in which the particles are assumed to be coupled by a magnetic field; however, a description of this work

is not included in this thesis. A derivation of the radial motion of the particle in the intense radiation field is given, including special and general relativity. This derivation is quite similar to that given by Abramowicz, Ellis and Lanza 1990. Next the solution of the wind equation under two different radiation stress energy tensors is shown. One of these cases was also used by Abramowicz, Ellis and Lanza 1990, and is presented for comparison with the other, new stress energy tensor devised by the author. A small change in the form of the stress energy tensor is shown to completely change the nature of the critical point solutions.

Finally, Chapter 10 describes the major results and conclusions of the thesis. The work which has not yet been done is also described here. Finally, the future prospects of X-ray astronomy are briefly described.

CHAPTER 2

X-RAY SPECTRA OF SEYFERT GALAXIES

General

As discussed in the previous chapter, many Seyfert galaxies and other emission line galaxies are observed in X-rays, and in fact emit a substantial fraction of their energy in X-rays. It has been found that the X-ray spectra from these galaxies have many similarities, and to date, at least five components have been identified which are common to the spectra of many Seyfert 1 nuclei. These are: (1) a power law continuum, (2) low energy absorption, (3) a soft excess component, (4) iron emission and absorption features around 7 keV, and (5) a hard tail. These features, the current state of observation and some theoretical models are reviewed in this chapter.

X-ray Power Law Emission

It has been found that the medium energy X-ray spectra of Seyfert 1 galaxies is generally well described by a power law. An early study by Mushotzky et al. (1980) performed with the A-2 experiment on-board *HEAO,1* found that the spectra of seven Seyfert 1 galaxies from 5-60 keV was well described by power laws with energy indices in the range 0.3 to 1.0, with the most common index found being 0.7. However, because of poor energy resolution, he found that most of these spectra could also be adequately fit with a high temperature thermal

bremsstrahlung model. A more sensitive survey of 48 Seyfert type AGN provided by EXOSAT showed that generally power law models provided better fits to the data than thermal bremsstrahlung models (see Chapter 3 for a description of the EXOSAT mission). The weighted mean index in this study was found to be 0.70, with 1σ dispersion of 0.17. It was noted also that there was a significant spread in the values of the index, beyond that expected for only statistical reasons (Turner and Pounds 1989). Another survey of *Ginga* data from 22 Seyfert 1 galaxies analyzed by Awaki (1991), found the average energy index to be 0.68 with the 1σ dispersion being 0.15 (see Chapter 6 for a description of the *Ginga* mission). Another sample of 29 *Ginga* spectra from 20 Seyferts found the mean index to be 0.722 with a standard deviation of 0.25 (Pounds, Nandra and Stewart 1990). Other surveys in medium energies (2–10 keV) seem to find a similar result (Turner et al. 1991). These results consistently show that the most common energy index is 0.7; however, the spread in values is too large to be entirely due to statistics, so there must be an intrinsic spread in the value of the energy index from object to object. This intrinsic spread may be due to differing emission mechanisms, or as discussed later in this chapter, could be due to the influence of additional broad spectral components.

The theory of the production of the power law X-ray emission is a topic of intense debate. Several mechanisms have been proposed.

A naturally promising mechanism involves synchrotron radiation, since it is a well known fact that an electron population with a power law energy distribution in a uniform magnetic field will produce a power law photon distribution. One particular model proposed is the synchrotron self-Compton model (Urry and Mushotzky 1982). In this process, radio to soft X-ray emission is synchrotron while the harder X-ray tail is due to Comptonization of the same synchrotron emission.

Another possibility is the Compton model. In this model, primary IR-O-UV soft photons are scattered by higher energy electrons to produce a power law spectrum. In some cases, the X-ray source shows high luminosity as well as fast variability. This implies that the source has a large compactness; in this case it is reasonable to expect that a significant population of electron-positron pairs would be present (e.g., Guilbert, Fabian and Rees 1983). Because of this expectation, many groups of theorists have investigated the spectrum of the radiation due to Comptonization in such electron-positron pair plasmas (e.g., Fabian et al. 1986; Lightman and Zdziarski 1987; Svensson 1987; Done and Fabian 1989). Their results in general indicate that an X-ray power law with an energy index of 0.7 might indeed be produced. However, a general concern with these models is that for a large region of parameter space, more γ -ray photons are produced than is consistent with the observed γ -ray background. This situation is particularly true if the observed energy index is to be 0.7. A way out of this dilemma may be the choice of realistic geometries. Recently, Tritz and Tsuruta (1991) have investigated a model in which the soft thermal emission is confined to a thin disk, and the reprocessing by Comptonization occurs in an electron-positron pair corona above the disk. Preliminary results indicate that indeed a power law with energy index of 0.7 might be produced without an over-abundance of γ -rays. Another way may be the addition of another hard X-ray spectral component with a harder spectrum to the steeper primary spectrum, modifying the measured power law index (Zdziarski et al. 1991). This point will be discussed later in this chapter.

Low Energy Absorption

The hard limit of the X-ray band pass measured depends usually on the detector used; that is, hard X-rays can in general be detected if the optical depth

of the detector is large enough. On the other hand, low energy photons are cut off due to an astronomical reason: they are easily photo-electrically absorbed by interstellar hydrogen, as well as heavier elements. A significant column density of interstellar material is present in our Galaxy. Column densities of this origin have been measured by their 21-cm hydrogen emission (Heiles 1975). The column number densities typically range from $1.0 \times 10^{20} \text{ cm}^{-2}$ to $3.0 \times 10^{21} \text{ cm}^{-2}$ in our line of sight to Seyfert galaxies considered in this thesis (Turner and Pounds 1989). In spectral fitting, the energy dependent absorption cross section is taken from Morrison and McCammon 1983, who include the effects of neutral heavy elements at cosmic abundances.

Many Seyfert 1 galaxies are not intrinsically heavily absorbed, and the absorption column as measured by spectral fitting is no larger than that due to our Galaxy. However, the results of a recent survey from EXOSAT showed that about half of 35 sources in which the absorption column could be measured showed significant absorption beyond that due to our Galaxy (Turner and Pounds 1989). Note that EXOSAT was a particularly good instrument to measure low energy absorption intrinsic to the host galaxy; because of its extended low energy detection, absorption columns down to 10^{20} cm^{-2} could be measured. There is also some evidence that, in general, high absorption columns are more common in low luminosity AGN (Reichert et al. 1985; Turner and Pounds 1989; Turner et al. 1991).

To clearly see the effect of the energy dependent absorption on the measured spectrum, in Figure 1 is shown the ideal spectra for various absorption columns. The dashed line shows the input spectrum with energy index of 0.7, while the solid lines show the emergent spectra. The numbers next to the emergent spectra give

Absorbed Spectra

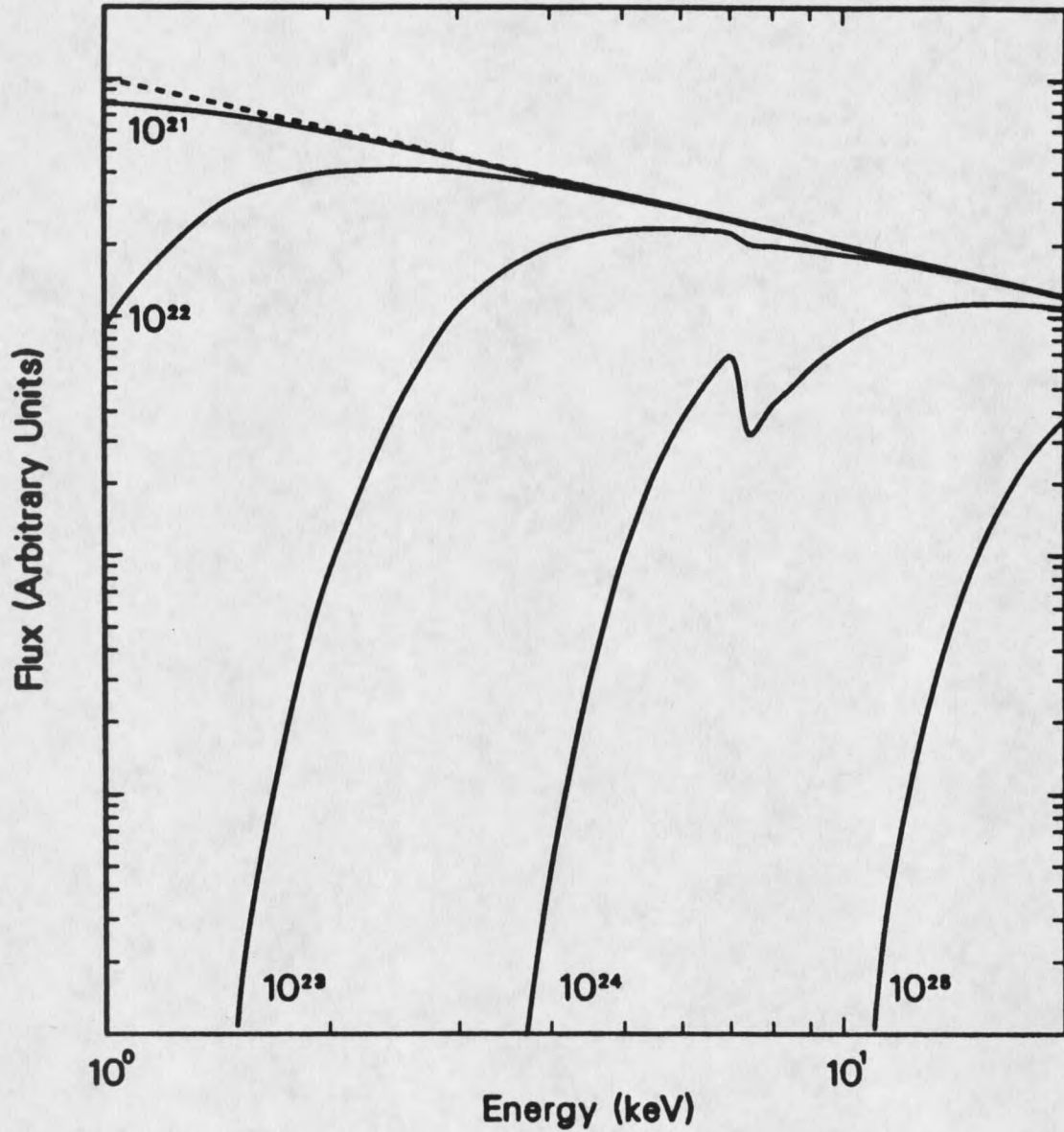


Figure 1. Absorbed spectra. Here the dashed line is the input spectrum with energy index 0.7, while the solid lines show the absorbed spectra. The figures by the solid lines give the absorption column densities in units of cm^{-2} .

the column density in units of cm^{-2} . As this figure illustrates, for columns above about 10^{23} cm^{-2} , the spectrum is quite heavily cut off at low energies.

In some cases there is evidence that the covering material is not uniform over the source, or that it is ionized and the ionization state is changing. These points will be discussed in Chapter 5.

Soft Excess Emission

Surveys performed with instruments having a band pass constrained to low energies have tended to measure steeper energy indices for power law models than those performed in the medium energy band. For example, a survey from the Imaging Proportional Counter on-board *Einstein* in the energy band from 0.2 to 4 keV finds an average index of 0.81 (Kruiper, Urry and Canizares 1990). The steeper index may be the result of an additional soft X-ray component, known as the soft excess. The EXOSAT spectral survey, taking advantage of the coverage of low and medium energy X-rays provided by the combination of the LE and ME experiments, found evidence for soft excess emission in approximately half of the unabsorbed sources (Turner and Pounds 1989). Because of the poor energy resolution of the LE instrument, these soft excess components could generally be fit with either an additional power law having an energy index in the range from 2 to 7, or with a thermal bremsstrahlung spectrum with kT of 0.15–0.4 keV. The detailed shape of the soft excess emission could not be determined.

The possibility that this excess is due to thermal emission has been investigated by theorists. It has been noted that excess emission known as the 'blue bump' is also found in the short wavelength ultraviolet continuum. Note that information from the extreme ultraviolet is not available due to interstellar photoelectric absorption, to the extent that the implied EUV excess cannot be directly

measured. However, in order to estimate the size of the excess, the two excesses have been fit by a variety of thermal models. For example, for Mkn 841, a single temperature blackbody fit to these excesses gives a luminosity of $2 \times 10^{46} \text{ erg s}^{-1}$ (Arnaud et al. 1985). This is an extremely large luminosity, and it would be super-Eddington for the range of black hole masses relevant for a Seyfert nucleus. Such a radiation field should cause the thin disk to blow up, making the argument inconsistent. Other theorists have proposed more realistic emission models (e.g. Sun and Malkan 1987; Czerny and Elvis 1987; Elvis, Czerny and Wilkes 1987) which may make this type of model more favorable.

Recently the data from the Solid State Spectrometer was re-analyzed simultaneously with data from the Monitor Proportional Counter on-board *Einstein*, and further evidence for soft excess emission was found. In fact, soft excesses were discovered in 46% of 26 sources studied (Turner et al. 1991). The higher resolution of the SSS and its low band pass (0.6–4 keV) combined with the wider band pass (1.2–20 keV) of the MPC made the measurement of the shape of the soft excess possible. The interesting result is that, in some cases, the soft excess measured was well fit by line emission rather than an additional power law or thermal bremsstrahlung. The interpretation was that the soft excess may be a blend of soft X-ray lines, rather than being thermal emission (Turner et al. 1991). This is an interesting result for several reasons. First, if the soft excess is not thermal in origin, the previously discussed problems with super-Eddington emission may be solved. Secondly, if this emission is due to soft X-ray lines, then the source of these lines, and the ionization state of the material emitting them must be identified.

Iron Emission and Absorption

For iron K-shell emission and absorption features to be observed in the hard X-ray spectra of Seyfert 1 galaxies, material in a relatively low state of ionization must exist which is illuminated by a substantial fraction of the continuum emission. The emission energy of the iron fluorescence line is not extremely sensitive to the ionization state for low states of ionization; however, the iron absorption edge energy is very sensitive (Makishima 1986). The least that must be true is that iron cannot be fully ionized, unless the iron line is due to recombination. However, the observed iron line energy from the better energy resolution data from *Ginga* indicates that the iron is not extremely ionized; in general, the iron must be more recombined than XVII. Such relatively recombined iron may be difficult to attain in the central region of an AGN unless the absorbing material is very dense. This is due to the extremely intense primary X-ray spectrum, which can completely ionize any iron atoms available, by photo-ionization. For example, a typical Seyfert galaxy may have an intrinsic luminosity of 10^{43} erg s $^{-1}$ in the X-ray band from 2–10 keV. Therefore, the flux available for photo-ionization may be at least an order of magnitude larger. Assuming a black hole mass of 10^7 solar masses, based on variability arguments, the Schwarzschild radius is $r_s \sim 3 \times 10^{12}$ cm. At least in one object (NGC 6814), the iron line flux has been found to vary in phase with the continuum X-ray flux (Kunieda et al. 1990). Therefore both the continuum and the line flux must be coming from the region of the central engine, taken for compactness arguments to be $\sim 10 - 100 r_s$. The ionization state of optically thin gas can be described by the ionization parameter ξ defined to be (Kallman and McCray 1982)

$$\xi = \frac{L}{nR_s} \cong \frac{10^{15}}{n} \quad (2.1)$$

where n is the number density. Now ξ must be less than ~ 1000 for iron not to be heavily ionized, and less than ~ 100 for oxygen to be an important contribution to the low energy opacity. For comparison, consider the Broad Line Region clouds, which lie outside the nucleus and have a typical density of $\sim 10^{10}\text{cm}^{-3}$. If they were inside the nucleus, ξ would be $\sim 10^5$ and iron would be completely ionized. On the other hand, if the density were $\sim 10^{15}\text{cm}^{-3}$, iron would be on the average unionized.

Can such dense gas exist in the central engine region of a Seyfert 1 galaxy? Guilbert and Rees (1988) demonstrated by a simple argument that such cool, extremely dense material necessary for iron emission might well exist in the central region of an AGN. This is because very dense material can easily cool by bremsstrahlung emission. In particular, if the accretion flow adopts a two phase configuration, and if the confining pressure is large enough to make the clouds dense enough, this process may be possible. Such a large confining pressure may be available from a magnetic field whose energy density is in equipartition with the gravitational potential energy of the infalling material (Rees 1987).

If cold material does exist in the central region, then iron emission features at ~ 6.5 keV are expected to be important spectral components because of several reasons. First, iron is relatively abundant, being 4.5×10^4 less abundant than hydrogen (Morrison and McCammon 1983). More importantly, the fluorescence yield for iron is relatively large. The K-shell electrons of lowly ionized iron can easily absorb an X-ray photon of energy equal to and somewhat greater than 7.1 keV. Because of their relative localization around the nucleus, the cross section of absorption is relatively large. This K-shell vacancy is readily filled by a L-shell or M-shell electron creating a fluorescence photon. If the electron comes from the L shell, then a K_α photon is born, with an energy of ~ 6.4 keV for iron less ionized

than XVII. If the electron comes from the M shell, the result is a K_β photon with an energy of ~ 7.1 keV. The radiation probability ratio of K_α/K_β is 0.135 (Weast 1975). As the ionization state of the iron becomes greater than XVII, the energy of the fluorescence photon also increases, becoming 6.7 keV for hydrogen-like iron (Makishima 1986). However, these photons do not always escape the atom. They may instead be absorbed by the atom causing the emission of an Auger electron. The fraction that does escape is known as the fluorescence yield, and iron has the highest fluorescence yield, being 0.34 (Bambynek 1972). Note that this is the fluorescence yield for neutral iron. If the iron is highly ionized, the fluorescence yield increases. For Fe XXIV, the yield is 0.75, for Fe XXV, the yield is 0.7, and for Fe XXVI, the yield is 0.5 (Krolik and Kallman 1987). Third, the iron emission line has energy of 6.4–6.7 keV and the iron edge has energy 7.1–9 keV, depending on the ionization state of the material (Makishima 1986). These features falls in the medium X-ray band where no other strong lines are expected. In contrast, emission lines due to lighter elements such as sulfur, oxygen, and neon, as well as the iron L emission line fall in the soft X-ray band; for example, the iron L line occurs at about 0.7 keV, the oxygen K_α line occurs at 0.52 keV, the neon K_α line occurs at 0.85 keV and the sulfur K_α line occurs at 2.3 keV. Therefore, because of its isolation, the iron line is more likely to be found by the spectral fitting of data from detectors with relatively low energy resolution.

If such cold material is available in the central region of the AGN, what would be the equivalent width of the iron line that might be expected to be measured? Recall that the line equivalent width is defined to be the width of the continuum flux band having the same flux as the line. If the emission arises from the fluorescence from material in the line of sight, the equivalent width will be quite small. For example for a column number density of 10^{22} cm $^{-2}$, and cosmic

abundances, the equivalent width is only about 10 eV (Makishima 1986). On the other hand, if the material is illuminated by the source and not in our line of sight, it can have a thicker column density than if it were in our line of sight. For example, a possible geometry is a flat thin accretion disk, which may be like a wall behind the source, being illuminated by the source. Then the solid angle being illuminated is 2π steradians, but the column density may be much larger, and therefore, the expected equivalent width is much larger. Monte-Carlo simulations indicate that the equivalent width in this situation might be as large as 200 eV, for a flat spectrum with a photon index of 1.4 when the disk system is viewed face on, falling to 0 when the disk is viewed nearly edge on (George and Fabian 1990). Note that the equivalent width has been found to be inversely correlated with the index, as expected (Awaki 1991). The equivalent width of the iron line can also be augmented if the continuum emission to our line of sight is somehow blocked, and we see preferentially the iron emission region (Makishima 1986). Such a situation might be the case in Seyfert 2 galaxies (Awaki 1991). In this case the equivalent width may be more than 1000 eV (Koyama 1989; Awaki 1991). However, very large equivalent widths from Seyfert 1 nuclei may be difficult to explain.

In some cases, the absorption edge due to iron can be measured. This can give some indication of the position of the iron emitting material, since material out of our line of sight with a given column density will show a much less deep edge than material with the same column in the line of sight. It can also indicate the relative abundance of iron in the central region. It is certainly possible to imagine that near the center of such an energetic object as an AGN, iron abundances may be enriched over the cosmic abundance value and in some cases, evidence for such a situation have been found (e.g. Holt et al. 1980). However, overabundance is generally an unattractive explanation, and such apparent overabundances can be

explained by geometry or ionization. For example, in some cases the iron edge energy may be measured. If the iron absorption edge has an energy much higher than the neutral edge energy, the contribution of a substantially ionized column is indicated.

The observations of the iron line around 7 keV are now many. Iron emission features have long been known to be present in the spectra of two bright active galaxies, Cen A (Mushotzky et al. 1978; Inoue 1985) and NGC 4151 (e.g. Warwick et al. 1989). Subsequently, the presence of these features has been discovered in the spectra of a Seyfert 1 nucleus, MCG-6-30-15, from a long observation by EXOSAT (Nandra et al. 1989). Iron features were also found in the spectrum of NGC 5506 from the long EXOSAT observation. This result will be described in Chapter 4. Recently, with the larger detector area on-board *Ginga*, iron emission lines were found to be common in Seyfert 1 nuclei (Awaki 1991; Nandra 1991). In the survey by Awaki (1991) sample of 22 Seyfert 1 galaxies were considered. Evidence for an iron emission line was found in all spectra. These features indicate the presence of neutral or partially ionized material being illuminated by the central continuum source. The equivalent widths measured ranged from 100 to 250 eV, with an average of 160 eV and a standard deviation of 60 eV. The study by Nandra (1991) of a sample of 29 spectra from 20 Seyferts found 26 line detections. In this sample the line energy was consistent with 6.4 keV. The average equivalent width found was 140 eV, with a standard deviation of 80 eV (Pounds, Nandra and Stewart 1991).

Note that in general a narrow Gaussian line ($\sigma = 0.05$ keV) provides usually an adequate fit to the *Ginga* spectra from Seyfert galaxies. This implies that, unlike the optical lines from the Broad Line Region, the material may not be in

rapid motion around the central black hole. Note that, however, the LAC on-board *Ginga* has the poor energy resolution characteristic of proportional counter detectors, and a small amount of broadening may not be detected. The width of the line has been constrained in only one case. This exception is NGC 4151, an exceptionally nearby Seyfert 1, in which the intrinsic width of the iron K_{α} line was found to be $\sim 38,000 \text{ km s}^{-1}$ FWHM, implying that the cold matter lies within 1 light day from the source (Yaqoob and Warwick 1991). Another exception is NGC 3227, a Seyfert 1 galaxy, from which an asymmetrical line was discovered (Pounds et al. 1989). This was subsequently modeled and interpreted to have been emitted from a rotating thin accretion disk, and subsequently to have been broadened due to gravitational redshift and Doppler shift (George, Nandra and Fabian 1990).

In one case, the iron emission line flux has been found to be variable. In NGC 6814, a 1989 *Ginga* observation found the line flux to vary in phase with the continuum flux, with the lag being less than 300 seconds (Kunieda et al. 1990). This observation places severe constraints on the position of the emitting gas, as discussed previously.

Hard X-ray Hump

The Large Area proportional Counter array on-board *Ginga* was the first X-ray detector to have both a large enough area and a large enough optical depth so that the spectra above 10 keV for Seyferts could be measured with fairly good resolution. The *Ginga* spectra from several Seyfert 1 nuclei seem to flatten at energies above ~ 10 keV. Detailed studies from several Seyfert 1 nuclei have found this result; included are MCG-6-30-15 (Nandra, Pounds and Stewart 1990; Matsuoka et al. 1990), NGC 4051 (Matsuoka et al. 1990; Kunieda et al. 1991); NGC

5548 (Nandra et al. 1991), NGC 7469 and IC4329A (Piro, Yamauchi and Mat-suoka 1990). Such a tail also was evident in the average of 12 *Ginga* spectra from Seyfert 1 nuclei (Pounds et al. 1990). In fact, a study by Nandra (1991) of 29 *Ginga* observations from 20 Seyferts finds the average of the 2–10 keV energy index to be 0.722, while the average of the 10–18 keV index is 0.37, and a statistical test finds the two index distributions to be different at greater than 99% confidence level (Pounds et al. 1991).

Theoretically, there are at least two explanations for the physical origin of the hard tail. These are the partial covering origin, and the reflection origin.

In the partial covering origin, a fraction of the primary X-rays is assumed to be occulted by a screen of thicker material. This screen can be in the form of clouds which cover the source (Poisson clouds), or in the form of a fraction of the source covered. Thus it is the sum of the two emissions which reach the observer. This model was proposed early to explain some aspects from the soft X-ray spectrum of NGC 4151 (Holt et al. 1980). In this case, the column density of the covered fraction is relatively small, typically $\sim 10^{22} \text{cm}^{-2}$. When this model is used to explain the hard tail above 10 keV, a denser column is needed. Figure 2 illustrates the partial covering model. The incident spectrum with energy index of 0.7 is shown by the dashed line. The spectrum from the covered component is shown by the dotted line. The column density of the covering cloud is $3 \times 10^{23} \text{cm}^{-2}$. The solid line gives the sum of the two components, where the normalization is such that 1/2 of the source would be covered. The spectral break is seen to be at around 9 or 10 keV, for this choice of covering column density and relative normalization.

Another possible origin of the hard tail emerges if the thick material illuminated by X-rays is behind the source instead of in front of it. That is, if very

